CLIMATE PATTERN RECOGNITION IN THE LATE HOLOCENE (1 AD TO 1150 AD, PART 6)

JOACHIM SEIFERT

FRANK LEMKE

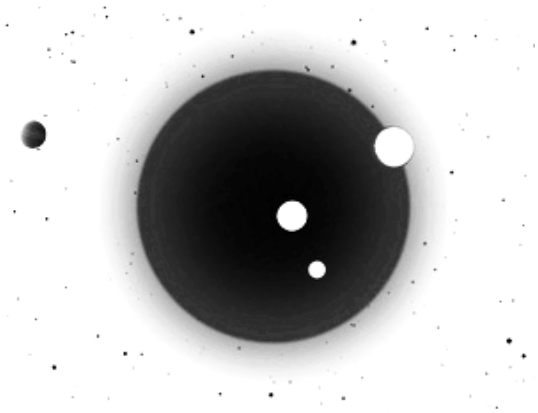

Correspondence to: weltklima@googlemail.com

Website: http://www.knowledgeminer.eu • http://www.climateprediction.eu

JANUARY 2017

Abstract. We continue to analyze each temperature spike within this time frame, using the Climate Pattern Recognition method, as explained in five previous Holocene papers, which commence with 8500 BC and which explain each single observed temperature rise and fall since this date. The analysis places its pattern recognition grid onto each time interval. The pattern grid consists of vertical lines for recurring Earth orbital periodicities, and of three more lines, which are horizontally inclined lines, i.e., the Milankovitch line and the upper and the lower orbital oscillation (EOO) boundary line. The Milankovitch line remained horizontal for six preceding BC millennia, now slowly turning into a descent towards the next glacial. The pattern recognition grid clearly identifies the swivel time span, required for the horizontal Milankovitch line to change into an inclined Milankovitch line with a descent trend of 0.47°C per millennium. The descending secular trend commences right within the first four AD centuries, known as RWP (Roman Warm Period). The RWP consists of twin temperature peaks, one at 115 BC and the second peak at 435 AD. Temperatures, from 435 AD on, start to fall significantly, as demanded by a threefold combination of the descending Milankovitch trend, the descent of the EOO-orbital sine line and of the descending part of the Z-shaped pattern of the 365 AD cosmic meteor impact. At 535-540 AD, additional cooling for two decades can be observed, the effect of the Ilopango volcano mega-eruption in El Salvador. As temperatures from 435 AD on rapidly descended, drought conditions set in, which greatly worsened living conditions on Earth. For this reason, the time after 435 AD is named as Dark Age Cold Period, Vandal Minimum or LALIA (Late Antique Little Ice Age), which led to the demise of a number of civilizations on Earth. In its progressing descent, cooling conditions worsened by two cosmic meteor impacts, Kanmare at 572 AD and Tabban at 680 AD. From the final temperature bottom of 751 AD, a vigorous temperature rebound set in, which is, after previous impact cooling, the second part of the Z-shaped cosmic impact pattern, visible in the GISP2 time series. This temperature rebound in a straight upswing graph line peaked in a high temperature spike, known as the Medieval Warm Period (MWP). This period occurred universally on the planet, because the Z-shaped cooling-warming-cooling pattern after each cosmic meteor impact is a global phenomenon on Earth. From the peak temperature in 1000 AD temperatures fell back to its pre-cosmic impact temperature level of 572-680 AD, now in 1100 AD, after forces of the two cosmic impacts have ultimately expired.

Citation. Seifert, J., Lemke, F.: Climate pattern recognition in the late Holocene (1 AD to 1150 AD, part 6), 2017, http://www.knowledgeminer.eu/climate_papers.html

1. APPLICATION OF THE PATTERN RECOGNITION GRID

In figure 1, the GISP2 temperature time series (Alley, 2000, 2004), transformed into equidistant time steps, and the selected time span of this paper is shown.

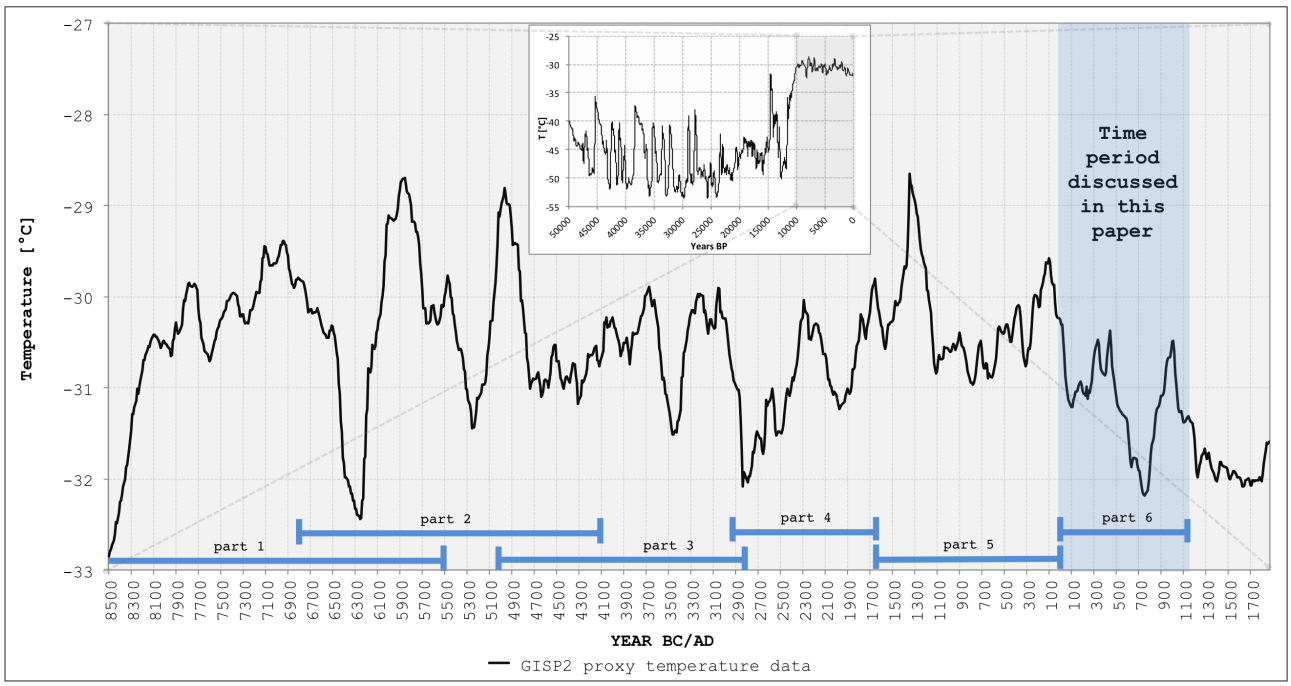

Figure 1. The Holocene GISP2 data (transformed into equidistant time steps) and the period discussed in this paper

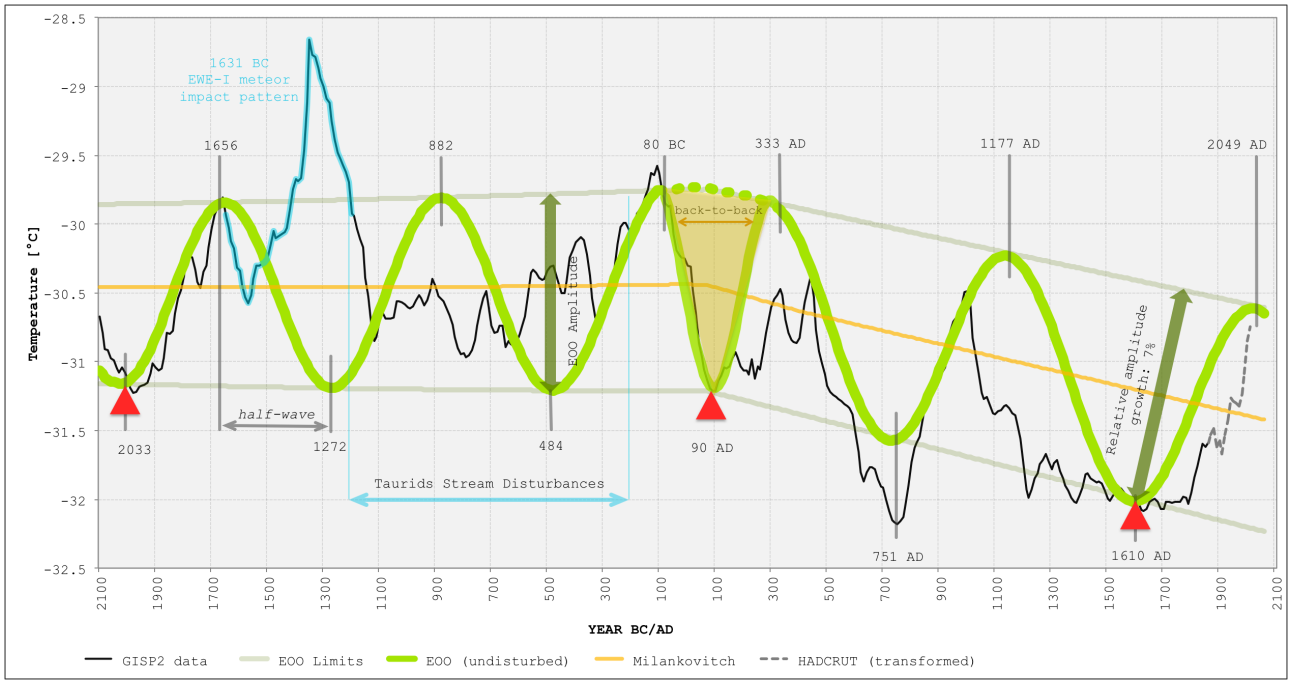

Figure 2. Superposition of Milankovitch and EOO climate drivers

When applying the grid to this time span the graph shown in figure 2 is obtained.

We start with the vertical periodicity lines of the grid, which, since 8114 BC, continuously increase in their length by 6.95 years for each successive period (half-waves). The term half-wave explains either a temperature movement upwards from the lower EOO (Earth Orbital Oscillation) level line to reach the upper EOO level line or, vice versa, a temperature movement from the upper EOO level down to the lower EOO level line. This movement is of astronomical origin, which continues unabated, but which is frequently masked by larger cosmic meteor impacts on Earth, which always influence the EOO and, therefore, alter the actual temperature course as noted in GISP2. In order to complete a full temperature sine wave with an up and down section, two half-wave periods together are needed. This applies for the entire Holocene. The dates of the beginning of half-waves (dates of vertical period lines) for the time span discussed in this paper are: BC 484, BC 80, AD 333, AD 751, AD 1177, AD 1610 and AD 2049.

Next, we focus on the grid's three horizontal lines. First, there is the central Milankovitch line, which represents the long-term temperature evolution, produced by the 100,000 years cycle, without the influence of all other climate forcing mechanisms. Above and below this line are the top and the bottom Earth orbital oscillation lines, which are the upper and the lower limit for temperature effects of regular Earth orbit oscillations (EOO). These three lines come in horizontally from the left over the past 6 millennia, but now, they turn downwards after 80 BC. In order to draw these three lines, we focus on the EOO bottom line, where three temperature minimum peaks are located, which remain unaltered by cosmic meteor impacts, which always reduce temperatures. Three triangles show those unaltered points (2033 BC, 90 AD, 1610 AD), which we connect as EOO bottom line. Thereafter, we determine the upper EOO-line with an upper EOO-point for the year 1610 AD and we measure the width of the EOO-amplitude at 484 BC and increase this value by 7%, to obtain the top marker point for the year 1610 AD. This method is possible, because periodicity length and periodicity amplitude are in linear relation, as calculated in (Seifert, 2010). The periodicity of the half-wave from 484-80 BC is 404 years, while during 1177-1610 AD it is 433 years, a gain of 7%. Therefore, the amplitude must be 7% wider. The third line is the Milankovitch line, which proceeds exactly in the center in between the upper and the lower EOO-line. We can do the fixation of both EOO-lines differently: Half-wave length and half-wave amplitude have a linear relation (Seifert, 2010). Therefore, we may calculate for any period their quotient and apply this quotient in the determination of all other periods and amplitudes. The resulting graph shows:

(1) Two back to back top peaks

(2) An entirely new low bottom peak, a pivotal turning point at 90 AD on the lower EOO-line

(3) Two half-waves; one downwards, 80 BC to 90 AD, the other upwards, 90 AD to 333 AD, which are compressed into one sole period, instead of occupying two periods, which is regular Holocene temperature evolution.

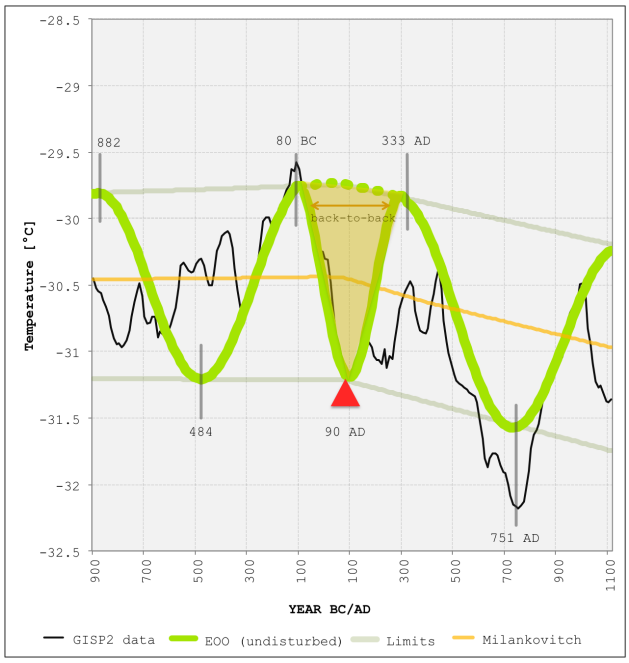

Figure 3. The Milankovitch line turning initiation

Obviously, the three features belong to one and the same cosmic process: the 100,000 year Milankovitch cycle of solar forcing. We show this new feature in a more detail in figure 3.

Remarkable is the temperature descend 80 BC to 90 AD, because this descend constitutes visibly the clean downward moving half-wave of the descent initiation pattern. It explains entirely this sharp and straight temperature drop over 150 years. No cosmic impacts occurred within this time span, to which this rapid temperature fall could be attributed. The compressed half-wave pattern placed two half-waves sections into only one period. This only is possible by producing steep temperature drop and recovery angles within the GISP2 temperature evolution.

For more explanation, we first need to discuss some features of the Milankovitch line: Plenty of literature exists on Milankovitch cycles, but no paper calculates and evaluates the long 100,000 (93,400) year cycle of the Sun movement, which is used within this pattern recognition analysis. All literature on the market concern short Earth movement cycles only, between 19,000 and 44,000 years in lengths, which we do not need, because they do not increase/decrease the distance between Sun and Earth, but only move angles in the orbital flight of Earth. Only a change in distance has the effect of receiving more/less incoming solar radiation on Earth, which then in turn raises, lowers or slightly turns the Milankovitch line in the GISP2 temperature graph.

The Sun´s movement, shown as downwards moving Milankovitch line, developed a pivotal point at 90 AD at the right hand side of the Milankovitch line, whereas on the left hand side, we see two complementing back-to-back peaks on the upper EOO line. These three points form a „triangular turn insert" into the regular grid system. Interesting is that the path of the Earth, in its orbital periodicity and orbital path amplitude remains unaffected by this Sun movement. This turning of the Milankovitch line from horizontal into a downward inclined trend line merits a separate paper on its detailed causes and mechanisms with its work title: „Climate Pattern Recognition: Solar forcing of the Glacial, the Interglacial (Holocene) and the return to the Glacial".

The new Milankovitch descent trend toward the next glacial is 0.47°C of GISP2 ice core degrees per millennium. Other proposed trends are 0.31°C, as determined by Jan Esper (Esper, 2012), based on Scandinavian tree ring measurements. Another value is about 0.4°C descent per millennium, of sea surface temperature, off the coast of Pakistan (Boell, 2014).

2. THE EFFECTS OF COSMIC METEOR IMPACTS ON GLOBAL CLIMATE

As we demonstrated in all previous papers, cosmic meteor impacts belong to the five major climate forcing mechanisms (fig. 4).

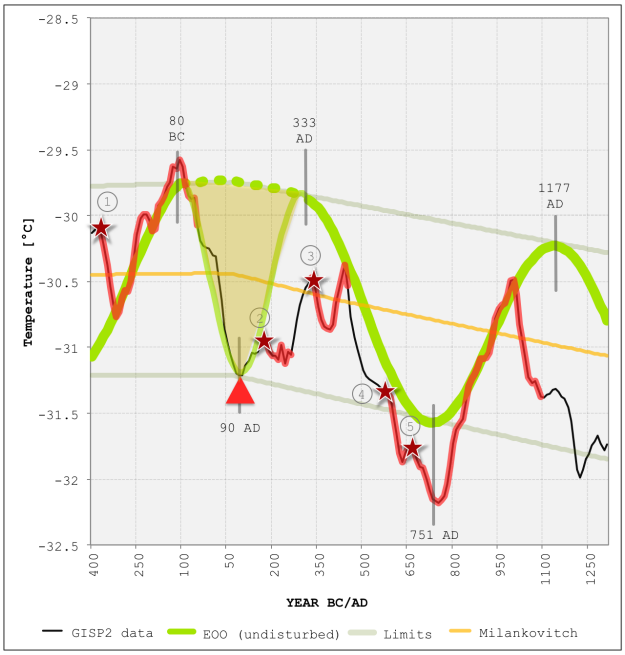

Figure 4. Cosmic meteor impacts
① *Helike*, ② *EWE-III*, ③ *Crete*, ④ *Kanmare*, ⑤ *Tabban*

We observe the following: All cosmic impacts, depending on impact bolide size, „mess up" a normal clean EOO-sine wave temperature evolution and produce Z-shaped cosmic impact patterns (Seifert, Lemke, 2012). The first event, on the left, (1), is the Helike impact of 373 BC, which was part of a Taurids Stream swarm which

additionally crossed China from March 1st to July 26, 368 BC, in 367 and in 366 BC. Those dates are recorded in Chinese Annals, pointing to metal raining from the sky.

There is one further small cosmic impact, clearly visible in GISP2 at 209 BC. A possible event candidate is the Chiemgau-Tuettensee impact in Bavaria (Ernstson, 2010) but the exact dating of the event remains still unresolved. Therefore this impact event location is rather a suggestion, by saying that the event took place in the first millennium BC. The impact could therefore have a different location.

The next cosmic impact events are: (2) the EWE-III impact and (3) the Crete impact, both of which stunted the development of a clean EOO-sine top of 333 AD and which produced a cut-off mini-temperature spike of 435 AD instead. Temperatures sharply fell from this 435 AD spike point. Harsh drought conditions accompanied this cooling. This combination of cooling and drought is a frequent feature in climate history. For example, focussing on the Nilometer in Cairo, which measured the water level of the Nile River 620-1300 AD (WaterHistory.org, 2016): We can see that the Nile water level continuously declined from 620 AD, the beginning of this record, until its bottom level in 750 AD.

Next, we recognize the dates of two more cosmic impacts (4) of 572 AD and (5) of 680 AD out of tree ring studies (Buentgen, 2016), as temperatures and precipitation steeply fall. The second, the 680 AD event, is also evident in Nilometer readings. Both, the (4) and (5) impacts, Kanmare and Tabban, sent temperatures to a level much lower than the regular bottom EOO-line. This EOO-bottom line constitutes the lowest possible temperature, without cosmic meteor impact forcing. From 750 AD, temperatures rebounded uninterrupted, in a straight line to its Z-shaped maximum peak in 1000 AD. From there on, temperatures reversed until 1100 AD, back to pre-Kanmare impact temperature levels of 572-680 AD.

3. ADDITIONAL DETAILS OF COSMIC METEOR IMPACTS

1. The Helike impact (373 BC) is described in the previous paper (Holocene part 5). The literature, for example, includes Lafond (Lafond, 1998).

2. The EWE-III Atlantic Ocean impact at 180 AD. The previous Holocene part 5 paper, described two previous Atlantic Ocean impacts, the EWE-I and II (Extreme Wave Events) in detail (Engel, 2013). Now, the EWE-III event is the last of three huge Atlantic mega-tsunami events with extreme-sized collapsing waves, which differentiates cosmic impact tsunamis from regular earthquake "long-wave" tsunamis. The background is that only meteor-induced tsunamis produce collapsing mega-waves of extreme height, capable to destroy shoreline morphologies, rip out and deposit dozens of tons weighing coral reef boulders onto high shore levels (Wuennemann, 2007). The EWE-III event should rather be called ECWE-III event (Extreme Collapsing Wave Event), which is not a less intensive tsunami, originating from sea quakes. This distinction is important, because an ECWE event is capable to deposit sea sand, shells and other maritime compounds onto the top of sea side cliffs in heights up to 200 m above sea levels, which no tsunami is capable. A collapsing wave event is therefore sufficient proof for an off-shore cosmic meteor impact.

3. The next cosmic impact occurred into the waters of the Eastern Mediterranean, West of Crete, July 21, 365 AD. The resulting mega-tsunami devastated most coastal towns in the Eastern Mediterranean: In Crete, Libya, Cyprus, and as far as Alexandria in Egypt. Most event literature does not consider the possibility of a cosmic meteor impact, all studies assume a plain seaquake; but one recent geological analysis of (Stiros, De Jevenois Acillona, 2012) shows that „a >70 km deep fault is necessary to match observed coastal changes … [but there is] ... no sign of a great tsunami generation fault south of Crete, existing in critical areas on the grounds of geology".

The mega-tsunami event was preceded by fierce lightening: The text of the Roman historian Ammianus Marcellinus (Marcellinus, 1862) says the following: „densitate praevia fulgurum acrius vibratorum tremefacta concutitur omnis terreni stabilitas ponderis…" i.e., „heralded by a thick succession of fiercely shaken thunderbolts" or in another translation: „preceded by incessant and furious lightening, the solidity of the whole ground was made to shake". The report does not use the term earthquake, „terrae motus", rather „acrius vibratorum". The cosmic impact occurred out in the open sea; impact fire columns were not visible from the land. But, as impact columns consist of a huge plume of burning dust, with temperatures up to 2200°C and reaching into stratospheric heights of more than 2000 km (Adushkin and Nemchinov, 2007), those fire dust compounds must have reached the Greenland ice. Ice analyses demonstrate two excessive peaks of fire tracers in Greenland ice over the past 3000 years: Both for the dates of the two great cosmic Northern Hemisphere impacts of 373 BC and of 365 AD. The three fire tracer substances are levoglucosan, carbon black and ammonia (Zennaro, 2014). Other types of terrestrial forest mega-fires determined in the ice only produce one-third or less of fire tracer contents.

To the wave propagation of the Crete impact mega-tsunami: Earth/seaquake induced tsunami produce long-waves, spreading in concentric circles, which distribute

the wave energy evenly into east and west. But this cosmic impact came in from the Northwest, pushing the highest waves to the Southeast, calculated to be 9.5 m height at Alexandria (Egypt), after a 110 min of wave travel towards the East, while on Sicily in the West, after a much shorter 60 min wave travel, waves were only half of the Alexandria height. This low Sicilian wave height occurred in spite of strong geological wave enhancing feature: A steep 30° degree „Malta escarpment," which rises 2 km high as rock front directly out of a deep Ionian abyss. Such escarpments produce much higher waves compared to a flat river coastlines, where waves run out as in Alexandria, in the Nile River delta.

The meteor crashed into the Mediterranean sea; the impact pressure onto the seafloor uplifted Western parts of Crete by 9 m. The NW-SE flight direction of the meteor appears in the shape of underwater homogenites-turbitides deposited on the Mediterranean Ridge in figure 1 of geological literature (Polonia, 2013). The underwater sediment turbitide composition has an unusual high Zr/Ti, Ca/Ti and Sr/Ti relation. A possible matching impact crater with a diameter of 10 km, could be the location of 34°19′37.64′′N and 20°03′38.62′′E.

4. The Kanmare impact, 572 AD, into the North Australian sea, described in detail by (Gusiakov, 2010), (Abbott, 2006), (Marto and Abbott 2006). The impact date is set to 572 AD +/- 86 years. We confirm the date by pointing to the extremely steep temperature drop, following the impact date, which is a major proof for any sizable meteor impact on Earth. The impact crater, underwater, is 18 km in diameter, thus quite large, which is the result of pressure propagation dynamics in the ocean. The cooling event is visible in the GISP2 record: The Kanmare impact sends temperatures into a free fall.

5. The next impact follows 110 years later: The Tabban impact of 680 AD. The literature of the Kanmare event usually groups the Tabban impact to the Kanmare impact. The Tabban event is evident in the GISP2 temperature graph: Temperatures fall steeply, to below the regular lower orbital boundary line.

4. RESUME FOR THE TIME SPAN OF THE LATE HOLOCENE, 1 AD-1150 AD

This time span started out as a large Z-shaped cosmic impact of 373 BC, with maximum temperature peak in 80 BC. The 550 year period (BC 115 to 435 AD) was termed Roman Warm Period (RWP). This Roman period is made up of two back-to-back periodicity maximum temperature peaks with the Milankovitch descent initiation period positioned in its center. The climate pattern recognition analysis exactly pinpoints this Milankovitch temperature descent initiation. No other Holocene model or simulation was capable to identify this feature. Starting out of the RWP descent initiation period, the Milankovitch trend line kept and still keeps falling by 0.47°C (Greenland borehole degrees) per millennium towards the next glacial. At the same time, the EOO-sine temperature line alternates around this Milankovitch trend line, forming maximum-minimum temperature peaks: The high temperature Roman Warm Period changes into a low temperature Dark Age Cold Period, followed by the high temperature Medieval Warm Period (MWP) and the cold Little Ice Age, from where on temperatures rise again into the Common Era Warm Period (CEWP), peaking 2049 AD. Both together, the Dark Age Cold Period and the Medieval Warm Period are joint features of a 550 year lasting Z-shaped cosmic impact pattern: Temperatures fell steeply after the 572 AD Kanmare impact to 750 AD (low temperature spike), rebounding steeply to 1000 AD (high temperature spike) and receded back again to pre-impact levels at 1100 AD. Thus, two cosmic impacts, Kanmare and Tabban, impeded the formation of an otherwise normally occurring, large rounded EOO-sine wave with its 1177 AD periodicity top. From 1 AD on, we encounter three possible types of warm temperature peaks: The first, the 333 AD peak of the RWP, appears as stunted cut off peak with a top remnant in 435 AD. The second, the regular EOO oscillation peak of 1177 AD, was converted to an earlier spike of 1000 AD by the two Kanmare and Tabban cosmic impacts. The third, the future 2049 AD CEWP peak, is not effected by any cosmic impacts, thus appearing as clean sine wave with a top plateau 2010 to 2070 AD.

The following part 7 paper will focus on the time span 550 AD to 2070 AD, and the last part of this series will analyze the period 1600 AD to the Holocene End.

REFERENCES

Abbott, D.H. et. al.: Impact craters as sources of megatsunami generated chevron dunes, paper nr. 119-120, GSA Philadelphia Annual Meeting (Oct 2006)

Adushkin, V. V., Nemchinov, I. V.: Catastrophic Events Caused by Cosmic Objects, Springer, 2007, pane 67 http://www.springer.com/us/book/9781402064517

Alley, R.B.: The Younger Dryas cold interval as viewed from central Greenland, Quaternary Science Reviews, Volume 19, Issues 1-5, 2000, http://www.ncdc.noaa.gov/paleo/icecore/greenland/greenland.html,

Alley, R.B.: GISP2 Ice Core Temperature and Accumulation Data. IGBP Pages/World Data Center for Paleoclimatology, Data ContributionSeries #2004-013, NOAA/NGDC Paleoclimatology Programs, Boulder, CO, USA

Ammianus Marcellinus, Roman History, London, Bohn (1862) Res Gestae, Book 26, chapter X, line 16, pp. 405-434

Boell, A. et.al.: Late Holocene primary productivity and sea surface temperature variations in the northeastern Arabian Sea: Implications for winter monsoon variability, Paleoceanography, 29, 778-794, doi: 10.1002/2013PA002579, AGU Publications 2014

Buentgen, U. et.al.: Cooling and societal change during the Late Antique Little Ice Age from 536 to around 660 AD, Nature Geoscience 9 (2016), 231-236, doi: 10.1038/ngeo2652, online: 8 Feb 2016

Engel, Max, et. al.: Holocene tsunamis in the Southern Caribian: Evidence from stratigraphic archives and the coarse-clast record, in: 4th International INQUA meeting on Paleoseismology, Active Tectonics and Archaeoseismology (PATA), 9-14 Oct 2013, Aachen, Germany

Ernstson, K. et al.: The Chiemgau Crater Strewnfield: Evidence of a Holocene large impact event in Southeast Bavaria, Germany, Journal of the Siberian Federal University, Engineering and Technologies 1, (2010, 3) p. 72-103, https://www.researchgate.net/publication/259471241_The_Chiemgau_Crater_Strewn_Field_Evidence_of_a_Holocene_Large_Impact_Event_in_Southeast_Bavaria_Germany

Esper, J.; et al.: Orbital foring of tree-ring data, Nature Climate Change (2012), doi: 10.1038/nclimate 1589
http://www.geo.uni-mainz.de/Dateien/Esper_2012_NatureCC.pdf and
http://www.nature.com/nclimate/journal/vaop/ncurrent/full/nclimate1589.html

Gusiakov, V.; Abbott, D.H.; Bryant, E.A.; Masse, W.B.: Megatsunamis of the world oceans: chevron dune formation, micro-ejecta and rapid climate change as the evidence of recent bolide impacts (2010), in: T.Beer (ed.) Geophysical Hazards, Springer Scienc and Business Media B.V., doi: 10.1007/978-90-481-3236-2_13
http://academiccommons.columbia.edu/download/fedora_content/download/ac:193311/CONTENT/Gusiakovetal_2009_Tsunami_Chevrons.pdf

Lafond, Yves (1998): Die Katastrophe von 373 v. Chr. und das Versinken der Stadt Helike in Achaia, in: Naturkatastrophen in der antiken Welt, Stuttgart, Steiner Verlag, ISBN 3-515-07252-7

Martos, S.; Abbott, D.H.: Impact spherules from the craters Kanmare and Tabban in the Gulf of Carpentaria, in: The Geological Society of America (GSA), the 2006 Philadelphia Annual Meeting, 22-25 Oct 2006, paper 118-119

Polonia, A.; et al.: Mediterranean megaturbitide triggered by the AD 365 Crete earthquake and tsunami, Nature Scientific Reports 3, article no 1285, 15.2.2013, doi: 10.1038/srep01285

Seifert, J.: Das Ende der globalen Erwärmung, Berechnung des Klimawandels, (2010), 109 pp., Pro Business Verlag Berlin, ISBN 978-3-86805-604-4, http://www.amazon.de/Das-Ende-globalen-Erwärmung-Klimawandels/dp/3868056041

Seifert, J., Lemke, F.: Five climate forcing mechanisms govern 20,000 years of climate change, 2012,
http://www.knowledgeminer.eu/climate_papers.html

Stiros, S.; De Jevenois Acillona, P.: The AD 365 giant earthquake and tsunami in the Eastern Mediterranean, Geophysical Research Abstracts, vol 14, EGU2012-4596, 2012, EGU General Assembly 2012, 22-27 April 2012, Vienna, Austria, p.4596

Wang, T.; Surge, D.; Walker, K.J.: Seasonal climate change across the Roman Warm Period/Vandal Minimum transition using isotope sclerochronology in archaeological shells and otoliths, Southern Florida, in: Quaternary International, vol. 308-309, 2. Oct. 2013, p. 230-341, Science Direct, Elsevier B.V.

WaterHistory.org: The Nilometer in Cairo
http://www.waterhistory.org/histories/cairo, last accessed December 2016

Wuennemann, K.; Weiss, R.; Hofmann, K.: Characteristics of oceanic-impact-induced large water waves - Reevaluation of the tsunami hazard, Meteorites and Planetary Science, 42, nr. 11, p.1893-1903 (2007), also:
https://www.researchgate.net/publication/227893553_Characteristics_of_oceanic_impact-induced_large_water_waves_-_Re-evaluation_of_the_tsunami_hazard

Zennaro, P., Kehrwald, N. et. al.: Fire in ice: two millennia of Northern Hemisphere fire history from the Greenland NEEM ice core, Clim.Past Discuss., 10, 809-957, 2014, http://www.clim-past-discuss.net/10/809/2014, doi: 10.5194/cpd-10-809-2014 and supplement doi: 10.5194/cp-10-1905-2014-supplement